Digest Journal of Nanomaterials and Biostructures Vol. 16, No. 4, October-December 2021, p. 1227-1234

Structural, optical characterization and photocatalytic behavior of Ag/TiO_2 nanofibers

Wu-Jhang Chen[#], Kuo-Chin Hsu[#], Te-Hua Fang[*], Chun-I Lee, Tao-Hsing Chen, Tung-Han Hsieh

Department of Mechanical Engineering, National Kaohsiung University of Science and Technology, Kaohsiung 80778, Taiwan

[#]*These authors contributed equally to this work.*

In this study, Ag doped TiO_2 nanofibers were successfully prepared by electrospinning technology for photocatalytic degradation. The structure, morphology and optical properties of the as-prepared nanofibers were analyzed through X-ray diffraction (XRD), field emission scanning electron microscope (FESEM), transmission electron microscope (TEM), and ultraviolet-visible spectroscopy (UV-Vis). Photocatalytic degradation results show that Ag doped TiO_2 nanofibers have higher photocatalytic activity than pure TiO_2 nanofibers under both visible light and ultraviolet light irradiation, which can effectively improve the degradation efficiency. The best degradation sample in this experiment is 5% Ag doped TiO_2 nanofibers, which can complete methylene blue (MB) degradation in 90 minutes under UV light and 70% MB degradation in 240 minutes under visible light.

(Received July 2, 2021; Accepted October 7, 2021)

Keywords: TiO_2, Electrospinning, Photocatalytic, Methylene blue

1. Introduction

With the development of industry and science technology, nano-crystalline semiconductor materials are widely used in corrosion resistance [1], light-emitting diodes [2, 3], solar cells [4-7], gas sensors [8-12], and photocatalysis [13-16]. The semiconductor materials used in photocatalysts are including TiO_2, ZnO, ZnS, WO_3, SnO_2, CdS, Fe_2O_3, and $BiFeO_3$ etc [16-24]. Among them, CdS and TiO_2 have the strongest photocatalytic ability, but CdS undergoes chemical and photochemical corrosion during the photocatalytic process [14]. TiO_2 is an n-type semiconductor, which has three crystal structures of anatase, rutile, and brookite, but only the anatase structure has photocatalytic properties [25].

The anatase structure TiO_2 has the characteristics of high oxidation energy, strong chemical stability, and non-toxicity, so it is one of the most promising photocatalyst materials. Since the energy gap of anatase phase TiO_2 is about 3.2 eV, in order to excite the electron of TiO_2 from the valence band to the conductive band, it is necessary to use ultraviolet light irradiation to process a photocatalytic reaction. Therefore, to improve the photocatalytic efficiency of TiO_2 under visible light is an important goal of recent research.

Usually, the main improvement method is to dope metal or non-metal in a matrix material to lower the energy levels of electronic transitions, so that the energy gap of TiO_2 is less than 3.2 eV, and visible light can be used to drive the TiO_2 photocatalyst to photodegrade MB aqueous solution. The main purpose of this research is to prepare one-dimensional Ag-doped TiO_2 nanofibers to make the energy gap less than 3.2 eV and improve the photocatalytic activity under visible light.

[*] Corresponding author: fang.tehua@msa.hinet.net

2. Experimental

In a typical experiment, the Ag/TiO_2/PVP (Poly(vinylpyrrolidone, Aldrich, Mw=1,300,000) solution was prepared by the following procedures: 1 mL of Titanium(IV) isopropoxide (99.99%, Aldrich), 2 mL acetic acid (99.7%, Aldrich), and 0.5 g of PVP were dissolved in 7 mL of ethanol (99.9%, Aldrich) to prepare the TiO_2/PVP precursor solution. $AgNO_3$ (99.98%, Aldrich) was added at different concentrations (0, 1, 3, 5, and 7%) to the TiO_2/PVP precursor solution. The above solutions were stirred for 12 h to obtain homogeneous solutions for electrospinning.

The electrospinning device consisted of a syringe and needle (21 Gauge, inner diameter = 0.514 mm), a syringe pump (Falco Tech Enterprise Co., Ltd. Taiwan), a high voltage power supply, and a collection board with heater. The optimal electrospinning parameters were a flow rate of 0.07 mL/h, and electrospun by applying 16 kV at a working distance of 15 cm. The composite fibers were collected then transferred to a combustion boat, and calcined at 550 °C for 4 h to remove PVP polymer in the air atmosphere.

The as-prepared Ag/TiO_2 nanofibers were characterized by FESEM (Hitachi SU8000, Japan), TEM (JEOL JEM-2100, Japan), and XRD analysis (Bruker D8 diffractometer using CuKα radiation). The thermogravimetric analysis (Mettler-Toledo, 2-HT) was conducted at a heating rate of 10℃ in the N_2 atmosphere from room temperature to 800℃. UV-Vis-NIR spectroscopy (UV-Vis-NIR, JASCO V670, USA) was used to measure the absorbance. The specific surface area of the TiO_2 and Ag/TiO_2 nanofibers was analyzed using Brunauer-Emmet-Teller (BET, Micromeritics Instrument Corp. Tristar II, Norcross, GA, USA).

The methylene blue (MB) solution (100 ppm) was used to evaluate the photodegradation efficiency of Ag/TiO_2 catalyst in visible light and ultraviolet light. The photocatalytic activity of MB solution was measured in a home-made photocatalytic reactor with a 75W Xe arc lamp equipped with a UV cutoff filter, and a 9W UV light source (Philips, wavelength = 365 nm). The MB solution was first stirred in the dark for 1 h for the photocatalysis tests and then use the UV–Vis spectroscopy to record the photodegradation of MB solution concentration.

3. Results and discussion

Fig 1(a) shows the TGA analysis of the as-prepared 7% Ag/TiO_2/PVP composite fibers. The total weight loss rate of the TGA curve is about 50.2%, which includes three stages of weight loss process. In the first stage, the weight loss was 11% from room temperature to 200°C, which was attributed to the evaporation of the volatile solvent and water content in the fibers. In the second stage, the weight loss from 200°C to 372°C was 14.9%, which was attributed to the gradual removal of PVP polymer from Ag/TiO_2/PVP composite fibers. However, in the final stage, a weight loss of 19.8% was observed from 372 to 500°C, which shows the maximum degradation of the PVP polymer. These results indicate that the entire organic compound is almost completely decomposed when the temperature reaches about 500°C. Therefore, the calcination temperature of this study was set as 550°C to ensure the organic compounds can be completely removed from the Ag/TiO_2/PVP composite nanofibers. Figure 1(b) shows the XRD pattern of TiO_2 nanofibers with different Ag contents after annealing at 550°C. XRD analysis indicates that the TiO_2 nanofibers are pure anatase phase and well agree with the JCPDS Card no. 21-1272. The XRD pattern of TiO_2 shows five primary peaks at 25.2°, 38°, 48.2°, 55°, and 62.5° which can be attributed to diffraction planes of anatase phase TiO_2 [15]. The Rutile and Brookite phases are not observed in these samples. However, we did not observe Ag diffraction peaks in Ag/TiO_2 samples. This phenomenon may be caused by the low content of doped Ag, and the strongest diffraction peak of Ag is covered by the diffraction peak of TiO_2 at 38°. Figure 1(c)~(g) shows the SEM images of 0, 1, 3, 5, and 7% Ag/TiO_2 nanofibers after annealing at 550°C. We found that the diameter of the pure TiO_2 nanofibers shown in Figure 1(c) is more uniform of about 140 nm. In Figure 1 (d) ~ (g), different amounts of Ag doped in TiO_2 fiber, the uniformity becomes worse and smaller nanofibers appear. All Ag-doped samples have a fiber diameter between 30 and 190 nm.

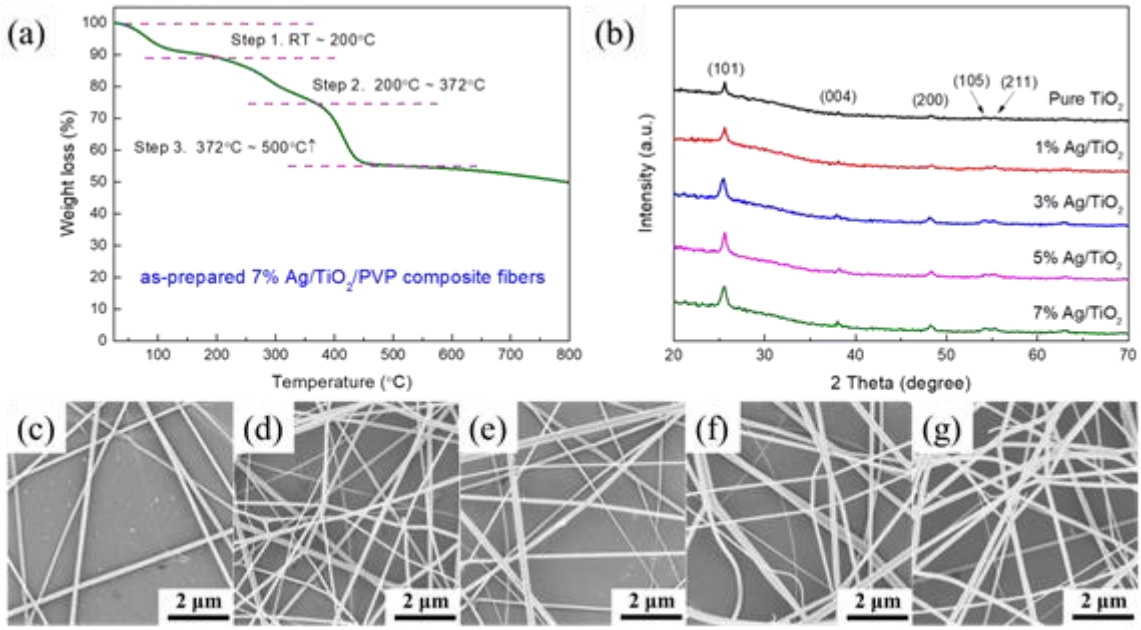

Fig. 1. (a) TGA analysis of the as-prepared 7% Ag/TiO_2/PVP composite fibers; (b) XRD, (c)~(g) SEM images of 0, 1, 3, 5, and 7% Ag/TiO_2 nanofibers after annealing at 550°C.

Figure 2 shows the TEM analysis of 7% Ag/TiO_2 nanofibers after annealing at 550°C. Figure 2(a) is low-resolution TEM images showing that the fiber diameter is about 80 nm. Figure 2(b) is high-resolution TEM images which can be observed that the lattice spacing is 0.35 and 0.23 nm corresponding to the TiO_2 (101) plane and Ag (111) plane, respectively. The results also indicated that the fibers prepared using electrospinning have good crystallinity. Figure 2(c) shows a selected-area diffraction pattern indicates that the Ag/TiO_2 nanofiber is a multi-crystalline structure. Fig. 2(d) is an Ag/TiO_2 single nanofiber mapping diagram, which confirms that the Ag particles are distributed on TiO_2 nanofiber.

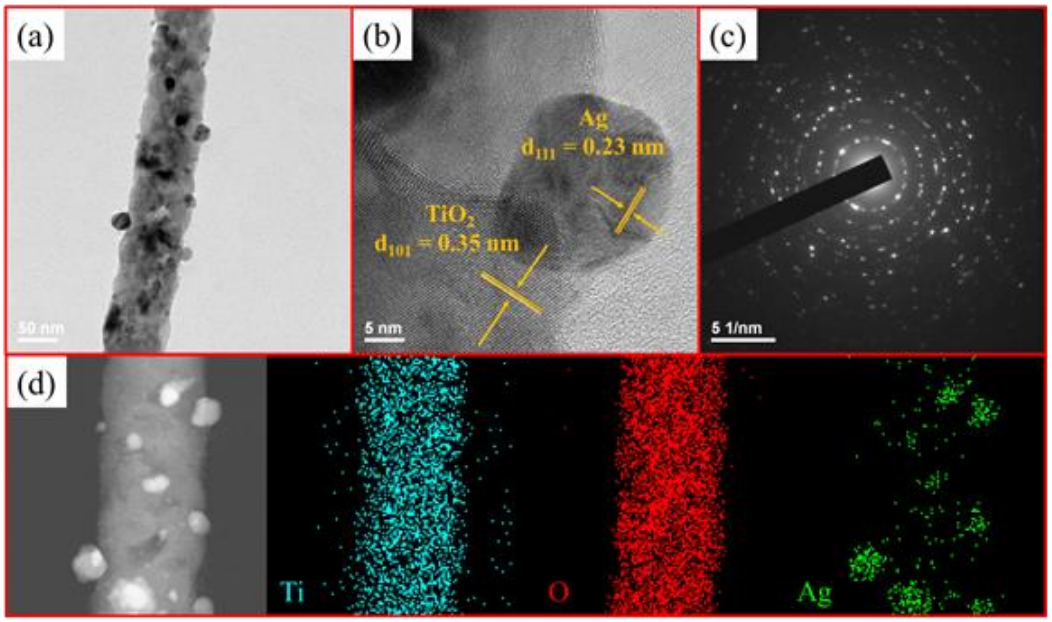

Fig. 2. (a) LR-TEM, (b) HR-TEM, (c) SAED, and (d) element mapping analysis of 7% Ag/TiO_2 nanofibers after annealing at 550°C.

The ultraviolet-visible absorption analysis of pure TiO_2 and Ag-doped TiO_2 nanofibers is shown in Figure 3(a). Compared with pure TiO_2 nanofibers, as the Ag content increases to 5%, the absorption in the visible light range increases, but when the Ag content increases to 7%, the absorption in the visible light range decreases slightly. The band gap energy of 7% Ag/TiO_2 nanofibers was calculated to be about 2.93 eV.

The XPS analysis of 7% Ag/TiO_2 nanofibers was shown in Fig. 3(b). The survey scan spectra showed that the peaks of Ti, O, C, and Ag can be detected and the C 1s caused by the PVP polymer remaining in the NFs. The results prove that the Ag element is doped in the TiO_2 nanofiber, which is consistent with Figure 2(d). Figure 3(c) and (d) shows the degradation of the Ag/TiO_2 nanofibers with different Ag content under visible light and ultraviolet light, respectively.

We found that Ag-added TiO_2 nanofibers have better catalytic degradation performance than pure TiO_2 nanofibers both under ultraviolet light and visible light. Among all the samples with Ag content, 5% Ag/TiO_2 nanofibers showed the best degradation. It only takes 90 minutes to complete the degradation of MB under ultraviolet light, and it can degrade 70% of MB in 240 minutes under visible light. The photocatalytic efficiency of 5% Ag/TiO_2 nanofibers has been investigated by measuring the decomposition of MB as a model pollutant under visible light and UV light irradiation. The oxidized and reduced forms of MB have different absorption bands in the UV-Vis spectrum. Therefore, we observed the progress of the decolorization reaction from MB to colorless MB by measuring the decrease in MB absorption in the UV-visible spectrum with a λ max of 664 nm. The time-dependent absorption spectrum of MB degradation during visible light and UV light irradiation are presented in Figure 3(e) and (f). After 90 min of irradiation under UV light in the presence of 5% Ag/TiO_2 nanofibers suspension, more than 99% of dye got degraded and the solution became colorless (insert in Fig. 3(f)). In addition, no new peaks appeared in the UV-Vis spectrum, which confirmed that there was no reaction intermediate during the degradation process. The results show that the photodegradation activity of Ag/TiO_2 nanofibers with heterostructure decreases significantly with time, and the best photodegradation efficiency is at 5% Ag content.

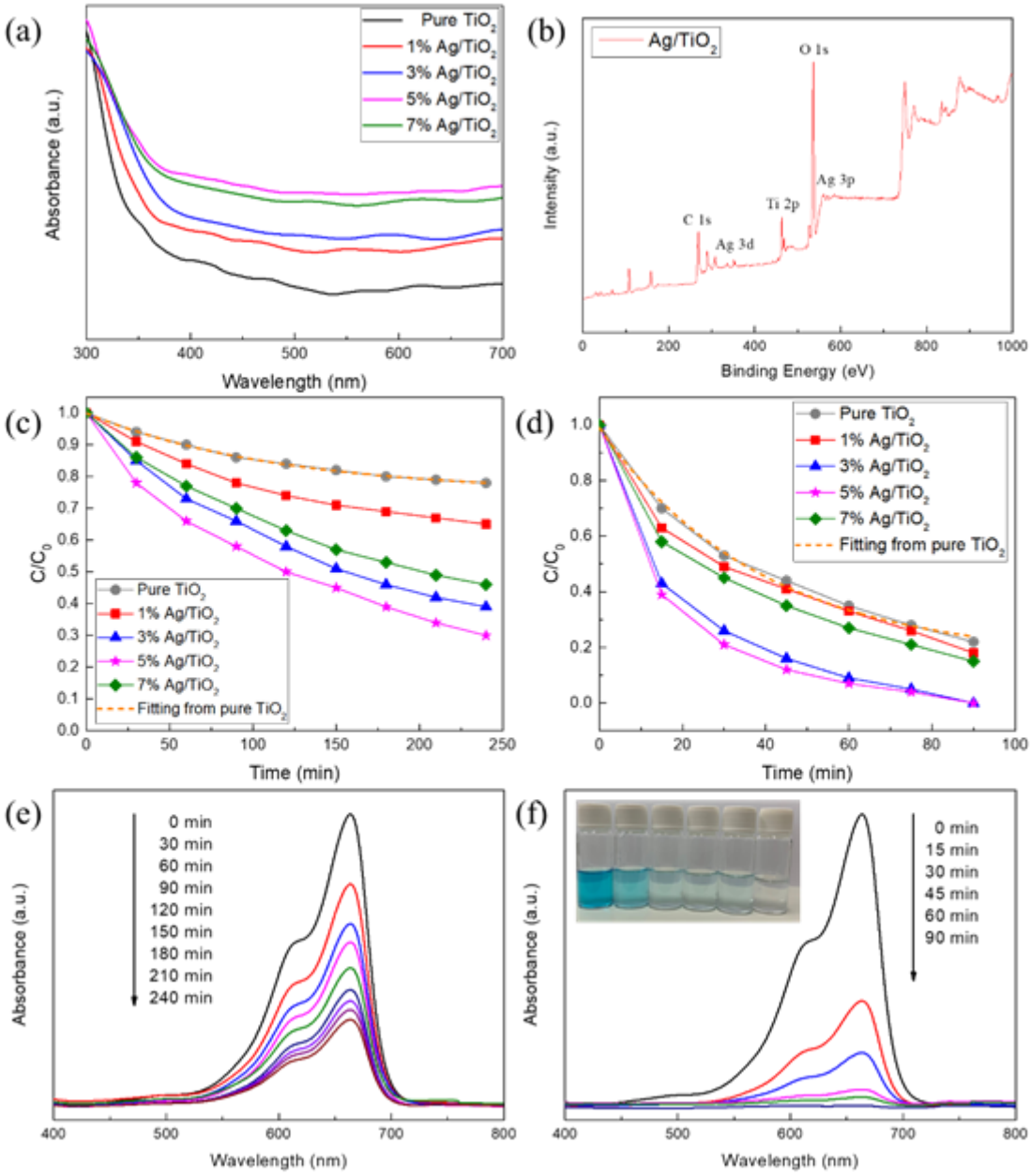

Fig. 3. (a) UV-Vis absorption analysis of different Ag-doped TiO_2 nanofibers; (b) XPS analysis of 7% Ag/TiO_2 nanofibers; Degradation of the Ag/TiO_2 nanofibers with different Ag content under (c) visible light and (d) ultraviolet light irradiation; The time-dependent absorption spectrum of MB degradation during (e) visible light and (f) UV light irradiation.

In addition, we use the exponential curve fitting method to obtain all the curves of the photodegradation data under ultraviolet and visible light, the equation of concentration reaction kinetics is as follow [15]:

$$\frac{C}{C_0} - k_0 = k_1 \cdot e^{-ht} \tag{1}$$

where k_0 is related to initial concentration, k_1 is a constant, h is related to the driving force of photodegradation, and its correlation coefficient R^2 are listed in table 1.

Table 1. The parameters for curve fitting equation.

Parameters	k_0		k_1		h		R^2	
Materials	**UV light**	**Visible light**	**UV light**	**Visible light**	**UV light**	**Visible light**	**UV light**	**Visible light**
Pure TiO_2	0.15684	0.74930	0.83191	0.24983	0.02576	0.00866	0.99380	0.99880
1% Ag/TiO_2	0.17045	0.60693	0.80811	0.39397	0.03061	0.00891	0.97671	0.99931
3% Ag/TiO_2	0.03492	0.24603	0.95389	0.74929	0.05192	0.00690	0.98967	0.99859
5% Ag/TiO_2	0.03067	0.21883	0.96223	0.76191	0.06020	0.00856	0.99293	0.99259
7% Ag/TiO_2	0.15283	0.32850	0.82786	0.66451	0.03596	0.00669	0.98072	0.99851
Pure TiO_2	0.15684	0.74930	0.83191	0.24983	0.02576	0.00866	0.99380	0.99880

We find that the correlation coefficients (R^2) of the exponential curves are all higher than first−order kinetics curves as shown in table 2. Therefore, the modified fitting curve can help to predict the C/C_0 value at each time during the degradation process.

Table 2. Comparison of correlation coefficients (R^2).

	R^2 (first-order kinetic)		**R^2 (modify curve fitting)**	
Materials	**UV light**	**Visible light**	**UV light**	**Visible light**
Pure TiO_2	0.97671	0.93183	0.99380	0.99880
1% Ag/TiO_2	0.97215	0.94022	0.97671	0.99931
3% Ag/TiO_2	0.97461	0.98874	0.98967	0.99859
5% Ag/TiO_2	0.97200	0.98854	0.99293	0.99259
7% Ag/TiO_2	0.97787	0.98581	0.98072	0.99851

4. Conclusion

In this study, Ag/TiO_2 nanofibers were successfully synthesized using the electrospinning method, for which the optimal Ag content was 5%. Compared with pure TiO_2 nanofibers, the Ag/TiO_2 nanofibers significantly improved photocatalytic degradation under both ultraviolet and visible light. The 5% Ag/TiO_2 nanofibers were able to degrade the MB solution in 90 minutes under ultraviolet light irradiation, and 70% of the concentration of MB solution could be degraded in 4 hours under visible light irradiation. Finally, the modified fitting curve can help to predict the C/C_0 value at each time during the degradation process.

Acknowledgments

The authors acknowledge the support in part by the Ministry of Science and Technology, Taiwan under grant number MOST 109-2221-E-992 -009 -MY3.

References

[1] C. -C. Li, T. -Y. Lai, T. -H. Fang, J. Nanosci. Nanotechnol. **20**, 6389 (2020).

[2] J. H. Park, D. Y. Kim, E. F. Schubert, J. Cho, J. K. Kim, ACS Energy Lett. **3**, 655 (2018).

[3] H. Qi, S. Wang, X. Jiang, Y. Fang, A. Wang, H. Shen, Z. Du, J. Mater. Chem. C **8**, 10160 (2020).

[4] K. -C. Hsu, J. -D. Liao, L. -M. Chao, Y. -S. Fu, Jpn. J. Appl. Phys. **52**, 061202 (2013).

[5] K. -C. Hsu, Y. -S. Fu, P. -Y. Lin, I. -T. Tang, J. -D. Liao, Int. J. Photoenergy **2013**, 156964 (2013).

[6] K. -C. Hsu, J. -D. Liao, J. -R. Yang, Y. -S. Fu, CrystEngComm, **15**, 4303 (2013).

[7] K. -C. Hsu, D. -Y. Wu, P. -Y. Lin, Y. -S. Fu, J. -D. Liao, J. Appl. Polym. Sci. **132**, 42388 (2015).

[8] K. -C. Hsu, T. -H. Fang, Y. -J. Hsiao, P. -C. Wu, J. Alloys Compd. **794**, 576 (2019).

[9] K. -C. Hsu, T. -H. Fang, Y. -J. Hsiao, Z. -J. Li, J. Alloys Compd. **852**, 157014 (2021).

[10] K. -C. Hsu, T. -H. Fang, I. -T. Tang, Y. -J. Hsiao, C. -Y. Chen, J. Alloys Compd. **822**, 153475 (2020).

[11] K. -C. Hsu, T. -H. Fang, S. -H. Chen, E. -Y. Kuo, Ceram. Int. **45**, 8744 (2019).

[12] K. -C. Hsu, T. -H. Fang, Y. -J. Hsiao, C. -A. Chan, Mater. Lett. **261**, 127144 (2020).

[13] R. Katal, S. Masudy-Panah, M. Tanhaei, M. H. D. A. Farahani, J. Hu, Chem. Eng. J. **384**, 123384 (2020).

[14] K. -C. Hsu, Y. -N. Chang, T. -H. Fang, T. -H. Chen, Y. -S. Fu, Mater. Res. Express **5**, 115507 (2018).

[15] K. -C. Hsu, T. -H. Fang, C. -I. Lee, T. -H. Chen, T. -H. Hsieh, Top. Catal. **63**, 956 (2020).

[16] S. M. Al-Shomar, W. R. Alahmad, Dig. J. Nanomater. Bios. **14**, 617 (2019).

[17] S. Sujinnapram, S. Nilphai, S. Moungsrijun, S. Krobthong, S. Wongrerkdee, Dig. J. Nanomater. Bios. **16**, 317 (2021).

[18] B. P. Reddy, V. Rajendar, M. C. Shekar, S. H. Park, Dig. J. Nanomater. Bios. **13**, 87 (2018).

[19] M. Javed, M. A. Abid, S. Hussain, D. Shahwar, S. Arshad, N. Ahmad, M. Arif, H. Khan, S. Nadeem, H. Raza, S. M. Harron, Dig. J. Nanomater. Bios. **15**, 1097 (2020).

[20] C. Zörer, O. Baytar, Ö. Şahin, S. Horoz, M. S. Izgı, Dig. J. Nanomater. Bios. **15**, 629 (2020).

[21] A. Modwi, B.R Y. Abdulkhair, M. E. Salih, N. Y. Elamin, A. M. Fatima, Dig. J. Nanomater. Bios. **14**, 357 (2019).

[22] C. Xu, P. R. Anusuyadevi, C. Aymonier, R. Luque, S. Marre, Chem. Soc. Rev. **48**, 3868 (2019).

[23] Y. Sun, E. D. Liu, L. Zhu, Y. Wen, Q. W. Tan, W. Feng, Dig. J. Nanomater. Bios. **14**, 463 (2019).

[24] Y. Sun, Q. Liu, L. Zhu, Q. W. Tan, Y. X. Fan, B. S. Zhao, J. Guo, Q. Q. Kong, Dig. J. Nanomater. Bios. **14**, 139 (2019).

[25] P. S. Basavarajappa, S. B. Patil, N. Ganganagappa, K. R. Reddy, A. V. Raghu, Ch. V. Reddy, Int. J. Hydrog. Energy **45**, 7764 (2020).